



Visible light driven (Fe, Cr)-codoped $\text{La}_2\text{Ti}_2\text{O}_7$ photocatalyst for efficient photocatalytic hydrogen production



Sujuan Hu ^a, Lichao Jia ^{a,b}, Bo Chi ^{a,*}, Jian Pu ^a, Li Jian ^a

^a Center for Fuel Cell Innovation, State Key Laboratory of Materials Processing and Die & Mould Technology, School of Materials Science and Engineering, Huazhong University of Science and Technology, Wuhan 430074, China

^b Fuels and Energy Technology Institute, Department of Chemical Engineering, Curtin University, Perth, WA 6102, Australia

HIGHLIGHTS

- (Fe, Cr)-codoped $\text{La}_2\text{Ti}_2\text{O}_7$ can increase the degree of narrowing of band gap.
- (Fe, Cr)-codoped $\text{La}_2\text{Ti}_2\text{O}_7$ exhibits excellent photocatalytic H_2 production of $360.203 \mu\text{mol g}^{-1} \text{h}^{-1}$.
- The calcination temperature and doping concentration are crucial for the photocatalyst.

ARTICLE INFO

Article history:

Received 28 January 2014

Received in revised form

9 May 2014

Accepted 12 May 2014

Available online 21 May 2014

Keywords:

Codoping

$\text{La}_2\text{Ti}_2\text{O}_7$

Photocatalytic H_2 production activity

Synergistic effect

ABSTRACT

Highly visible-light response (Fe, Cr)-codoped $\text{La}_2\text{Ti}_2\text{O}_7$ photocatalysts are synthesized by sol-gel process. The crystal phase, morphology and optical absorption activity of the samples are characterized by X-ray diffraction, scanning electron microscope, X-ray photoelectron spectroscopy, and UV-vis diffuse reflectance spectra. The results reveal that the calcination temperature and dopant concentration have strong influence on the phase structures, crystallinity and morphology. The UV-vis diffuse reflectance spectra indicate that Fe and Cr ions codoping can extend optical absorption to the visible-light region and narrow the band gap obviously. The photocatalytic hydrogen and oxygen production activities are evaluated in CH_3OH and AgNO_3 aqueous solution under solar light irradiation. NiO_x (0.5 wt%) loaded (Fe, Cr)-0.005-LTO-1150 shows the best photocatalytic H_2 production activity with the productivity of $360.203 \mu\text{mol g}^{-1} \text{h}^{-1}$ and the apparent quantum efficiency of 2.44%, which suggests that the synergistic effect of Fe and Cr codoping is favorable to enhance the photocatalytic efficiency. The photocurrent of (Fe, Cr)-codoped $\text{La}_2\text{Ti}_2\text{O}_7$ is more than two times of that for Fe-doped $\text{La}_2\text{Ti}_2\text{O}_7$ photocatalyst. The efficient photocatalytic hydrogen production and the high photocurrent of (Fe, Cr)-0.005-LTO-1150 are originated from the optimized combination of the physical-chemical properties, the small band gap and the low recombination rate of photoelectron-holes.

© 2014 Elsevier B.V. All rights reserved.

1. Introduction

The production of H_2 by solar energy conversion has been considered as one of the strategies to solve fossil fuel exhausting. Since Fujishima and Honda first reported photo-electrochemical splitting water on TiO_2 electrodes in 1972 [1], photocatalytic splitting water into H_2 over semiconductor photocatalysts using solar irradiation has attracted a lot of attentions [2–6]. Since then many

efforts have been put into modifying semiconductor photocatalysts to improve the hydrogen production activity under visible light. Perovskite-type lanthanide titanate ($\text{La}_2\text{Ti}_2\text{O}_7$, LTO) is a promising photocatalyst for photocatalytic H_2 production because of its layered structure and unique electronic configuration [7–9]. However, the large band gap (ca. 3.8 eV) of $\text{La}_2\text{Ti}_2\text{O}_7$ prevents its applications in visible light, which possesses 43% of the solar energy, thus reducing the efficiency of the photocatalytic H_2 production significantly and limiting its practical application [10,11]. To solve this disadvantage, various strategies have been developed to narrow the width of the band gap of photocatalysts for maximum utilizing solar energy over recent decades [12,13]. An efficient method to extend the range of light absorption is to substitute the Ti sites in the perovskite-type $\text{La}_2\text{Ti}_2\text{O}_7$ with the doping metal elements, such as Fe^{3+} or Cu^{2+} .

* Corresponding authors. Center for Fuel Cell Innovation, State Key Laboratory of Materials Processing and Die & Mould Technology, School of Materials Science and Engineering, Huazhong University of Science and Technology, Wuhan 430074, China. Tel./fax: +86 27 87558142.

E-mail addresses: jialc@hust.edu.cn (L. Jia), chibo@hust.edu.cn (B. Chi).

[14–16]. However, monodoped photocatalysts usually do not favor efficient photocatalysis due to the limited decrease in band gap, in addition, the introduced unoccupied impurity states in the forbidden gap are proved to be the recombination centers for photoelectron–holes [17,18]. Recently, researchers experimentally and theoretically suggested that two or even more metal elements codoping is a promising method to improve photocatalytic H₂ production activity of the photocatalyst, because codoping can be beneficial to keep charge balance in the codoping system, improve the migration of carriers within the band gap, and further increase the degree of narrowing of band gap than monodoping [19–21]. That is, host photocatalyst with the synergistic effect of the multiple metal elements codoping can show the best photocatalytic activity for water splitting. For instance, Zhang reported that (Ag, La)-codoped CaTiO₃ showed effective photocatalytic H₂ production ability [22]. Jia suggested that the codoping of SrTiO₃ with Ni and La could lead to the obvious narrowing of the band gap and greatly improve the photocatalytic activity under visible irradiation [23]. Long adopted a hybrid density functional theory approach to discuss the synergistic effect in gap engineering of double-cation-impurity-doped anatase-titania [17].

Besides, recent studies demonstrated that photocatalytic H₂ production activities of La₂Ti₂O₇ photocatalyst are strongly depended on its phase structures, crystallinity, surface defects and morphology [24–30], which are affected remarkably by calcination temperature and doping concentration [23]. For example, Hwang and co-workers reported that the doped metal elements could be inserted into the lattice of the monoclinic La₂Ti₂O₇ photocatalyst and the crystallinity is improved when calcined at a high temperature [12].

In this study, we give detail investigation about (Fe, Cr)-codoped La₂Ti₂O₇ photocatalyst for optical absorption and photocatalytic H₂ production activity, which is seldom studied up to now. The focus of our work is to investigate the synergistic effect of Fe and Cr codoping on the photocatalytic H₂ production activity of La₂Ti₂O₇ photocatalyst. The electronic structures were calculated for understanding the nature of band structure for Cr and Fe codoped La₂Ti₂O₇. Moreover, the effect of the calcination temperature and the codoping concentration on the physical–chemical properties, including phase structures, crystallinity and morphology, and photocatalytic H₂ production activities are also studied in detail.

2. Experimental

2.1. Preparation of photocatalysts

(Fe, Cr)-codoped La₂Ti₂O₇ photocatalyst powders were synthesized by sol–gel method [12]. In a typical procedure, 13.67 g of tetrabutyl titanate (Ti(OCH₃)₄) was first dissolved in 88.93 g of ethylene glycol to form solution A; then 84 g of citric acid was dissolved in 80 mL of distilled water to form solution B. And then solution B was added into solution A under continuous stirring. After mixing homogeneously, 17.32 g La(NO₃)₃·6H₂O and the required amount of Fe(NO₃)₃·9H₂O and Cr(NO₃)₃·9H₂O were added. The molar percent of Cr and Fe corresponding to Ti is set as 0.0025 (C₁), 0.005 (C₂), 0.01 (C₃), 0.02 (C₄) and 0.03 (C₅), respectively. The final mixture solution was stirred for 2 h at 50 °C in an open system by oil bath until it became a transparent clear solution. Then it was heated at 130 °C for 8 h for facilitating esterification between ethylene glycol and citric acid. The solution was concentrated to obtain the precursor. The precursor was calcined at 350 °C for 4 h and milled to obtain the black powders. The final powder samples were obtained by calcining the black powders at 850 (T₁), 950 (T₂), 1050 (T₃), 1150 (T₄) and 1250 °C (T₅), respectively, for 2 h. The synthesized photocatalysts were marked as (Fe, Cr)–C_x–T_y, where C_x and T_y denote the codoped concentration and calcined temperature, respectively. The Fe- and Cr-doped La₂Ti₂O₇ and pure La₂Ti₂O₇ were also synthesized for comparison using the same route. The loading of 0.5 wt% NiO_x cocatalyst was conducted by stewing photocatalyst in Ni(NO₃)₂ solution and then H₂ reduction at 500 °C for 2 h followed by oxidation at 200 °C for 1 h [31].

2.2. Characterization

The crystal phases of synthesized photocatalysts were determined by X-ray diffractometer (XRD, X'Pert pro. PANalytical B.V) with a Cu K α radiation. The microstructure was detected by the field emission scanning electron microscopy (FE-SEM, FEI, Sirion 200). Chemical composition and the states of the elements were detected by X-ray photoelectron spectroscopy (KRATOS AXIS165 X-ray photoelectron spectrometer). The UV–vis diffuse reflectance spectra were recorded with a Perkin–Elmer Lambda 35 UV–vis spectrophotometer.

2.3. Photocatalytic activity

The photocatalytic H₂ production was performed in a closed quartz reactor under 500 W xenon lamp (100 mW cm⁻², CHF-XM 500, Beijing Trusttech Co., Ltd.) irradiation in methanol aqueous solution (25 vol %) accompanied with continuous magnetic stirrer. For comparison, the photocatalytic O₂ evolution of the photocatalyst in AgNO₃ aqueous solution (0.01 M) was also conducted under same condition. Before photocatalytic experiments, the reaction vessel was evacuated for 30 min to remove the dissolved oxygen and ensure the anaerobic conditions. The amount of evolved gases were analyzed by an on-line gas chromatography (DongXi GC-A5000, high purity argon as a carrier gas) equipped with a thermal conductivity detector and 5 Å chromatographic column. The apparent quantum efficiency (AQE) was measured under the same photocatalytic reaction conditions. The focused intensity and areas on the flask for xenon lamp was ca. 100 mW cm⁻² and 19 cm², respectively. The AQE was calculated according to the following equation:

$$\text{AQE [\%]} = \frac{\text{number of reacted electrons}}{\text{number of incident photons}} \times 100 \\ = \frac{\text{number of evolved H}_2 \text{ molecules} \times 2}{\text{number of incident photons}} \times 100$$

2.4. Photo-electrochemical measurement

The working electrodes were prepared as follows: 0.2 g of photocatalyst was grinded with 0.06 g polyethylene glycol (PEG, molecular weight: 20,000) and 0.5 mL water to make a slurry. The slurry was then coated onto a 2 cm × 1.5 cm FTO glass electrode by the doctor-blade method. And the resulting electrodes were dried and calcined at 450 °C for 30 min. Photocurrents were measured using an electrochemical analyzer (Zennium, Zahner) with a standard three-electrode system using the prepared samples as working electrodes, a platinum plate as counter electrode, and Ag/AgCl (saturated KCl) as a reference electrode. And 1 M Na₂SO₄ aqueous solution was used as the electrolyte [32–33].

3. Results and discussion

3.1. Crystal structure

Fig. 1 shows XRD patterns of pure and (Fe, Cr)-codoped La₂Ti₂O₇ photocatalysts. The patterns of pure La₂Ti₂O₇ can be indexed to the

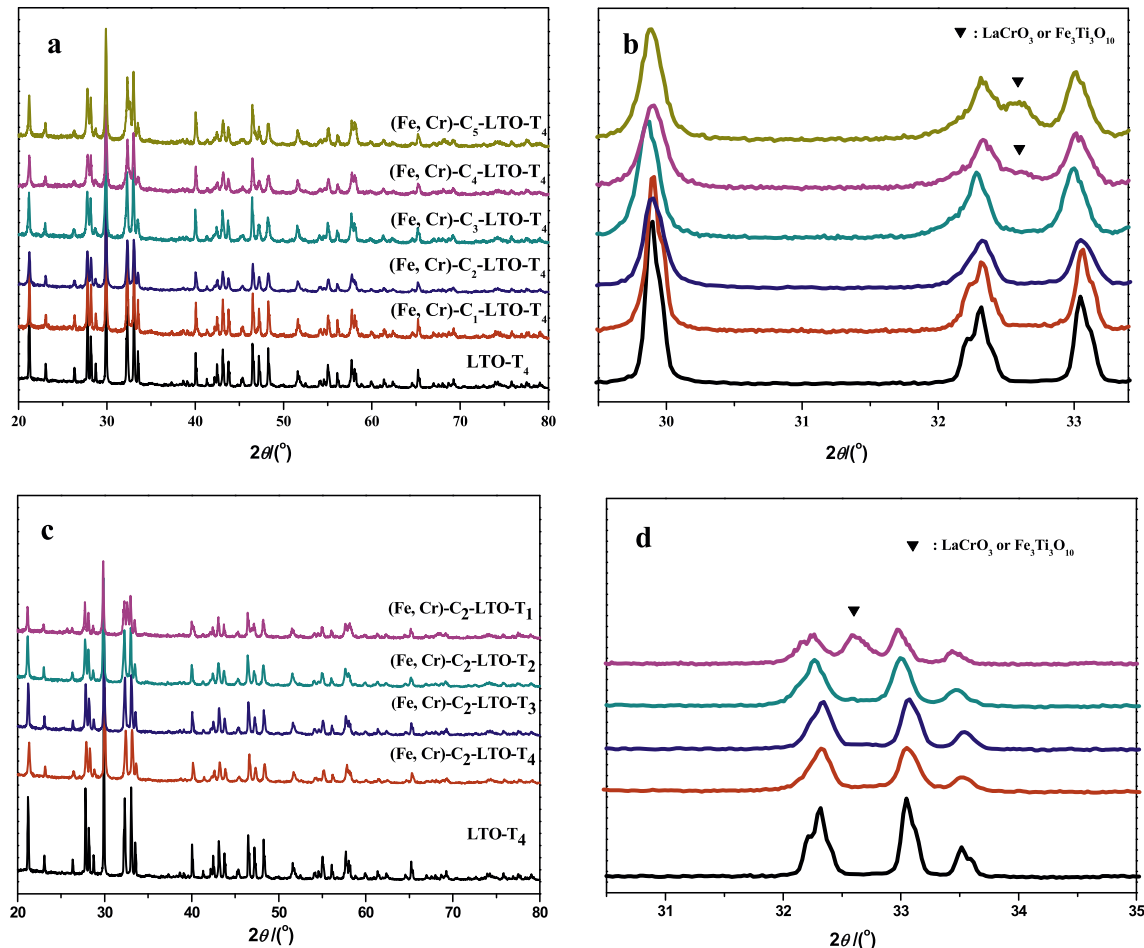


Fig. 1. X-ray diffraction patterns of (Fe, Cr)-C_x-LTO-T₄ (a) and X-ray diffraction peaks from 29.5° to 33.5° (b), X-ray diffraction patterns of (Fe, Cr)-C₂-LTO-T_y (c) and X-ray diffraction peaks from 30.5° to 35° (d).

La₂Ti₂O₇ monoclinic structure, and no impurities are detected [JCPDS: 28-0517]. It is clear that the crystallinity of La₂Ti₂O₇ has a slight decline with the codopants concentration increasing (Fig. 1a). And when the doping concentration of Fe and Cr concentration is less than 0.01, no other impure phases indicating of Fe or Cr compounds can be found, indicating that Fe and Cr cations may have been incorporated into the La₂Ti₂O₇ lattice. However, the diffraction peaks assigned to orthorhombic LaCrO₃ or Fe₃Ti₃O₁₀ appear when Fe and Cr dopants concentration higher than 0.02 (Fig. 1b), in addition, the intensity of the impurity phase increases with the codopants concentration [16]. The same impurity peak can also appear when calcination temperature below 950 °C (Fig. 1c and d). Since the cationic radius of Ti (0.605 Å) is between the radii of Fe (0.645 Å) and Cr (0.530 Å), the doping of Cr and Fe into Ti site in the lattice will not result in the obvious change of the lattice parameter. Due to the large radii size difference between Fe, Cr and La (1.180 Å), the doping of Fe and Cr into La site will bring obvious lattice shrinkage on XRD patterns. However, from XRD results we can find no obvious change of lattice shrinkage of expansion can be observed and also no impurity of phase including Fe and Cr is found. Thus, the possible sites of Fe and Cr in the lattice are to replace Ti site other than La site.

3.2. Morphology

The morphologies of pure and (Fe, Cr)-codoped La₂Ti₂O₇ photocatalysts are studied by SEM (shown in Fig. 2). For pure La₂Ti₂O₇

(Fig. 2a), irregular structure can be observed. While for the codoped samples calcined at different temperature (Fig. 2b–e), it can be seen that the particles sizes of the codoped samples are smaller than those of the pure La₂Ti₂O₇ in general. This is because the codoping can introduce crystal defects, which would inhibit the growth of the crystal [34,35]. The result also shows that with the increase of the calcination temperature, the particles sizes become larger and the morphology becomes more homogeneous. Usually, high temperature is favorable to the crystallinity of perovskite-type crystalline grains. However, it also will cause large particle size [23]. Fig. 2f, g and h (with 0.0025, 0.01 and 0.03 codoped concentration) show the morphologies of La₂Ti₂O₇ with different Fe and Cr concentrations. It can be observed that the codopant concentration shows apparent effect on the morphology and some small particles are formed at a high codoped concentration.

3.3. XPS analysis

The chemical states of Ti, O, La, Cr and Fe species in (Fe,Cr)-C₂-LTO-T₄ photocatalyst were investigated by the XPS technique, as shown in Fig. 3. C 1s region was used as reference for correcting spectra for the charge accumulation. It can be seen that Ti 2p displays a doublet peak centered at 457.89 and 463.62 eV, respectively, which originates from the spin orbital splitting of 2p_{3/2} and 2p_{1/2} states [36]. The core level of Ti 2p XPS spectra exhibits shifting towards lower binding energies (BEs) compared with tetravalent Ti (TiO₂ BE: 2p_{3/2} 458.9 eV, 2p_{1/2} 464.6 eV) [37].

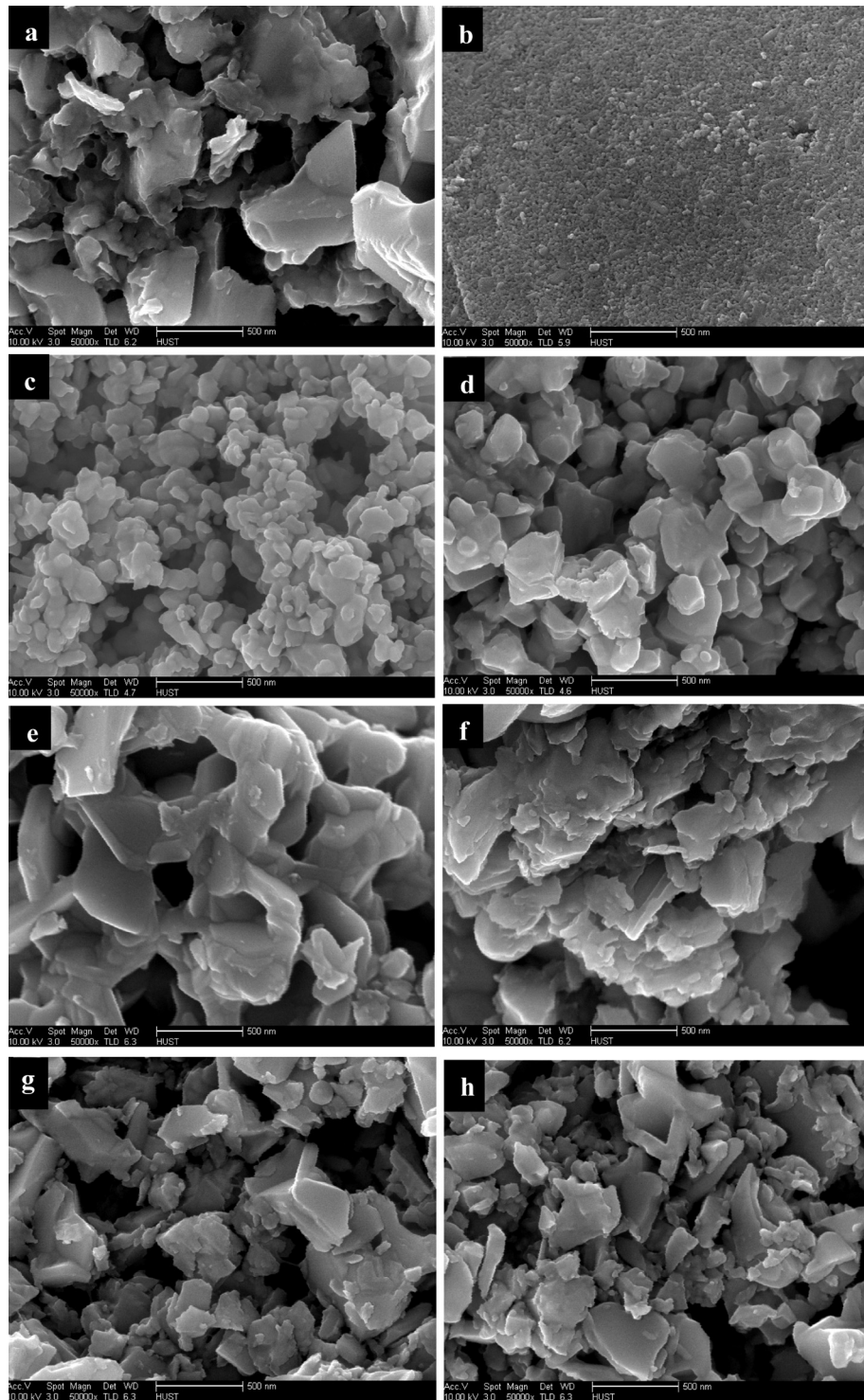


Fig. 2. SEM images of pure $\text{La}_2\text{Ti}_2\text{O}_7$ (a), (Fe, Cr)– $\text{C}_2\text{-LTO-T}_y$ (T_1 (b), T_2 (c) and T_3 (d) and T_5 (e)) and (Fe, Cr)– $\text{C}_x\text{-LTO-T}_4$ (C_1 (f), C_3 (g) and C_5 (h)).

It is well known that doping can lead to the formation of oxygen vacancies and Ti^{3+} defects and result in a slight shift of the Ti 2p peaks toward the lower binding energy [38,39]. Hence, the shift of the Ti 2p peak can be assigned to the Fe and Cr element doping effect of the TiO_2 lattice. O 1s region is fitted with two peaks centered at 529.30 and 531.59 eV. The first peak is assigned to lattice oxygen and the second may be attributed to surface adsorbed oxygen (O^-) [37]. A complex multi-peak structure is

observed in the La 3d core level spectra. Seven peaks at 833.73, 838.13, 850.54, 855.00, 836.26, 852.96 and 846.22 eV are observed for La 3d. These peaks originate from the spin orbital splitting of $3\text{d}_{5/2}$ and $3\text{d}_{3/2}$ states, which agree well with the values of trivalent La [40,41]. The peaks at 576.73 and 586.30 eV can be assigned to shake-up satellites of $\text{Cr} 2\text{p}_{3/2}$ and $\text{Cr} 2\text{p}_{1/2}$, respectively. Two peaks at 580.12 and 589.57 eV, which can be assigned to $\text{Cr}^{6+} 2\text{p}_{3/2}$ and $\text{Cr}^{6+} 2\text{p}_{1/2}$, are found in Fig. 3d [42].

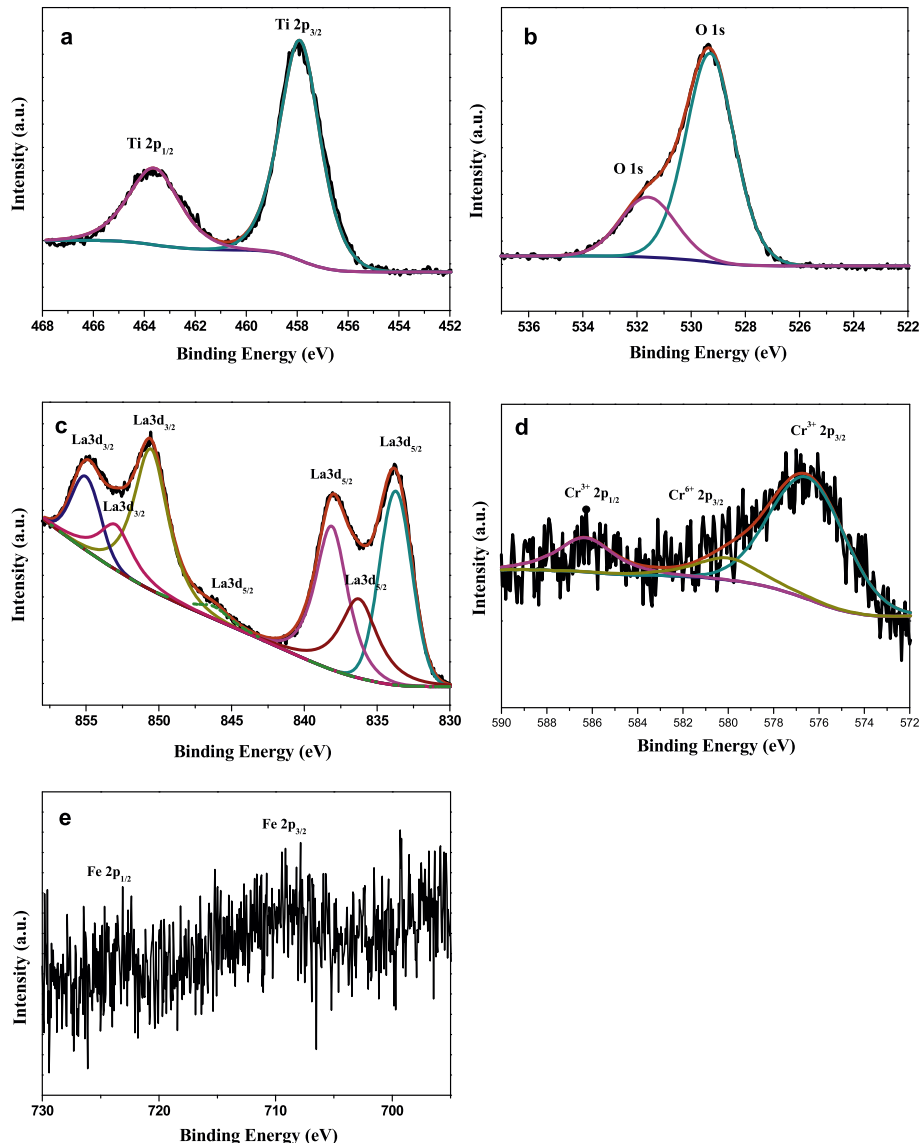


Fig. 3. XPS spectra for Ti 2p (a), O 1s (b), La 3d (c) Cr 2p (d) and Fe 2p (e) regions of (Fe, Cr)-C₃-LTO-T₄.

The formation of Cr⁶⁺ is beneficial to keep charge balance in the codoped system. To be specific, partial Cr atoms release two more electrons than Ti atoms to the La₂Ti₂O₇ lattice and may act as electron donor, while Fe atoms and other Cr atoms release one less electron than Ti atoms and may act as electron acceptor. If the electrons on the donor levels passivate to the same extent as the holes on the acceptor levels, charge-compensated n-p doping pairs are forming [17]. This mechanism is favorable to inhibit the formation of the defects and oxygen vacancies that generally play an undesirable role as the recombination center of photogenerated electron-hole pairs during the photocatalytic reaction. XPS spectra for Fe 2p are not obvious, however, two peaks at 709.80 and 723.61 eV can be found. The two peaks originate from the spin orbital splitting of 2p_{3/2} and 2p_{1/2} states, which can be assigned to Fe³⁺ (Fe₂O₃ BE: Fe 2p_{3/2} 710.8 eV, Fe 2p_{1/2} 724 eV) [43]. The binding energies of Cr³⁺ (Cr 2p_{3/2}: 576.73 eV and Cr 2p_{1/2}: 586.30 eV) and Fe³⁺ (Fe 2p_{3/2}: 709.80 eV and Fe 2p_{1/2}: 723.61 eV) show obvious shifts compared with their metal oxide (Cr₂O₃: Cr 2p_{3/2} 576.10 eV, Cr 2p_{1/2} 586.00 eV and Fe₂O₃: Fe 2p_{3/2} 710.8 eV, Fe 2p_{1/2} 724 eV), which may be due to

the formation of Ti—O—Cr and Ti—O—Fe bonds after the doping of Cr³⁺ and Fe³⁺ into TiO₆ lattice. Moreover, according to the excess monoclinic octahedral TiO₆ stabilization energy for Fe and Cr ions, they should occupy preferentially the octahedral TiO₆ sites in the perovskite structure [44]. And other researchers have also proved that the stable solid solutions such as La₂Ti₂O₇, SrTiO₃ and CrTiO₃ could be formed via partial substitutions of Ti sites by Cr³⁺ and Fe³⁺ (up to 10%) [45,46].

3.4. UV-vis absorption

Fig. 4 displays the UV-vis diffuse reflectance spectra of pure, monodoped and (Fe, Cr)-codoped La₂Ti₂O₇ photocatalysts. Pure La₂Ti₂O₇ can only respond to the UV-light and shows no optical absorption property in the visible-light region, while the optical absorption region of (Fe, Cr)-codoped La₂Ti₂O₇ has been extended to the visible-light region. The enhanced optical absorption property is greatly related with the codoped concentration. Specifically, the optical absorption scopes of La₂Ti₂O₇ with 0.0025, 0.005 and 0.01 codoped concentration are nearly similar. In contrast,

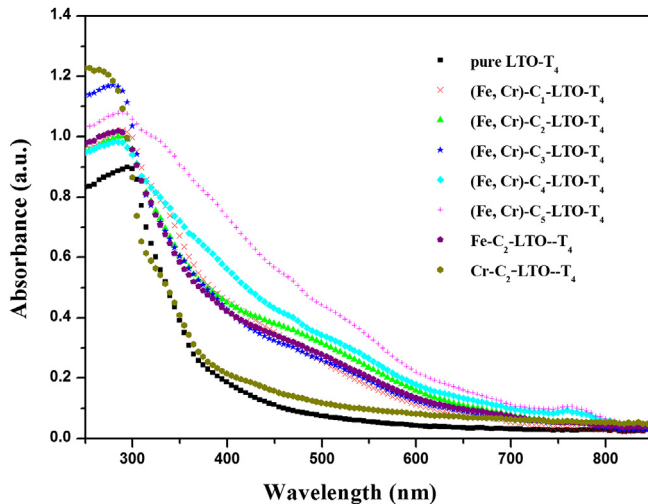


Fig. 4. UV-vis diffuse reflectance spectra of pure, monodoped and (Fe, Cr)-codoped $\text{La}_2\text{Ti}_2\text{O}_7$.

optical absorption scope and strength are further enlarged and a small absorption peak in the range 740–800 nm has appeared with 0.02 and 0.03 codoped concentration. The red-shift of the optical absorption edge and the appeared small absorption peaks can be ascribed to a d–d transition ${}^4\text{A}_2 \rightarrow {}^4\text{T}_2$ in Fe^{3+} or Cr^{3+} [47]. Moreover, Fe and Cr ions codoping have induced a series of impurity states (Fe 3d and Cr 3d orbital) in the forbidden gap of $\text{La}_2\text{Ti}_2\text{O}_7$. The electrons of Fe 3d4s and Cr 3d4s are easily excited from the valence band (VB) to the conduction band (CB) over $\text{La}_2\text{Ti}_2\text{O}_7$ under the visible-light irradiation, which can lead to the broad optical absorption in the visible-light region.

3.5. Calculation of electronic structure

The electronic structures of pure, monodoped $\text{La}_2\text{Ti}_2\text{O}_7$ and (Fe, Cr)-codoped with Fe and Cr at the Ti site are calculated by using projected augmented wave (PAW) method [48], as implemented in the Vienna *ab-initio* simulation package (VASP) [49–51]. For doping cases, a $1 \times 1 \times 2$ supercell with 88 atoms is used, where dopant complexes are substituting on the Ti site. In order to obtain the band gap that is consistent with the experimental results, the so-called GGA + U method with $U = 6.3$ eV for Ti 3d state is employed, due to the well-known limitation of GGA [52]. Accordingly, the calculated band gap of undoped is $\text{La}_2\text{Ti}_2\text{O}_7$ is 3.68 eV, which is in good agreement with the experimental value of 3.80 eV. The total density of states (TDOS) and projected density of states (PDOS) are plotted in Fig. 5 for all the considered systems. As can be seen from Fig. 5a, for the undoped system, the valence band maximum (VBM) is dominated by O 2p state, while the conduction band minimum (CBM) by Ti 3d state. For Fe-doped $\text{La}_2\text{Ti}_2\text{O}_7$ (Fig. 5b), two kinds of impure bands from Fe 3d states are located in the band gap: one is above the VBM and the other is below the CBM. The most significant feature for Cr-doped $\text{La}_2\text{Ti}_2\text{O}_7$ (Fig. 5c) is the formation of a new band of Cr 3d states. However, the band gaps of both the two mono-doped systems do not change, regardless of the impure energy levels. The impure states can be served as the springboard of the photoexcited carrier transition: the electrons in the valence band can be excited into gap states and subsequently to the conduction band under visible-light irradiation. For (Fe, Cr)-codoped $\text{La}_2\text{Ti}_2\text{O}_7$ (Fig. 5d), the band gap is narrowed to 2.83 eV due to the overlap of doped states and the VBM. Meanwhile the hybridized states

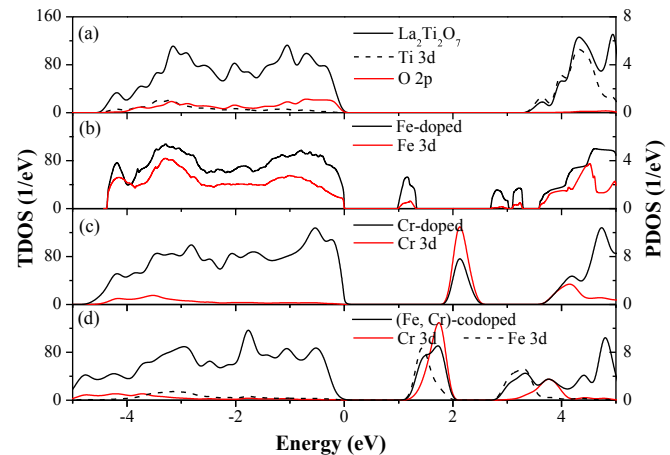


Fig. 5. Calculated TDOS and PDOS of pure (a), monodoped (b, c) and codoped (d).

arise from O 2p, Fe 3d and Cr 3d states which favor the migration of photoexcited carriers, locate in the band gap. The hybridized states and narrowed band gap indicate that the codoped system may have better photocatalytic activity than the monodoped systems.

3.6. Photocatalytic H_2 production activity

The photocatalytic H_2 production activity from water splitting under solar light irradiation is measured and the results are shown in Fig. 6. It has been reported that NiO_x is an excellent cocatalyst that could boost the photocatalytic H_2 production activity, since it can efficiently promote the separation of the photogenerated electron–hole pairs [12]. Pure $\text{La}_2\text{Ti}_2\text{O}_7$ photocatalyst has large band gap (ca. 3.8 eV) and exhibits low photocatalytic activity in H_2 production from water splitting under solar light irradiation. The H_2 evolution rate has been improved with increasing calcination temperature to a maximum value of $360.203 \mu\text{mol g}^{-1} \text{ h}^{-1}$ with an apparent quantum efficiency (AQE) of 2.44% for the codoped sample calcined at 1150°C , which is 24 times higher than the undoped $\text{La}_2\text{Ti}_2\text{O}_7$, 5.7 times higher than Fe-doped $\text{La}_2\text{Ti}_2\text{O}_7$ photocatalyst and 2.3 times higher than Cr-doped $\text{La}_2\text{Ti}_2\text{O}_7$ photocatalyst as shown in Fig. 6a. Furthermore, the calcination temperature shows important effect on the performance of H_2 evolution. The H_2 evolution rate for sample calcined at 1150°C is almost 33 times higher than that calcined at 850°C . Fig. 6c shows the photocatalytic H_2 production activities of (Fe, Cr)-codoped $\text{La}_2\text{Ti}_2\text{O}_7$ photocatalysts with different codopant concentration. Photocatalytic H_2 production activities of the codoped samples reach the maximum with Fe and Cr concentration of 0.005. When the codopant concentration is lower than the optimal concentration of 0.005, the capture traps of charge carriers in the photocatalyst is insufficient, thus the photocatalytic H_2 production activity will be enhanced with the increasing of codopant concentration. However, when the codopant is excessive of the optimized concentration, the recombination of the charges will be increased. Furthermore, the high doping concentration can also lead to the enrichment of the doped ions on the surface of photocatalyst, causing a decrease of photocatalytic H_2 production activity.

For comparison, Fig. 7 also shows photocatalytic O_2 evolution of the photocatalysts. Sample (Fe, Cr)-C₄-LTO-T₄ shows the highest photocatalytic O_2 evolution performance, compared with the highest H_2 evolution activity in (Fe, Cr)-C₂-LTO-T₄. This different is

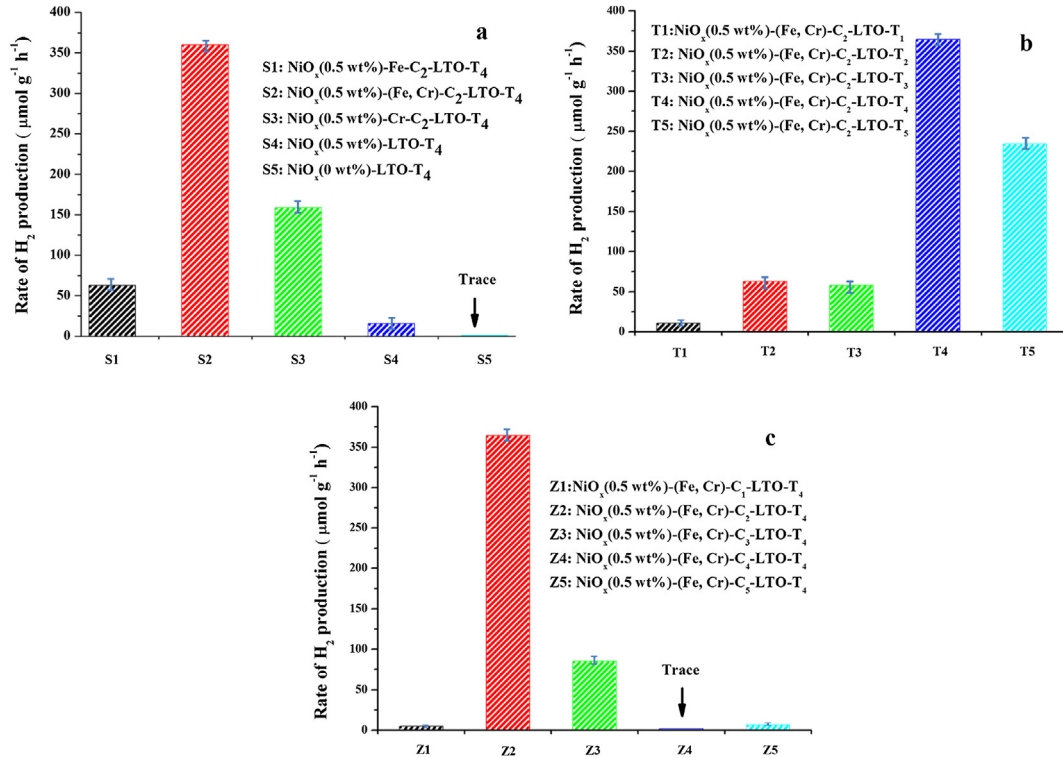


Fig. 6. Photocatalytic H₂ production of pure, monodoped and codoped (a), (Fe, Cr)-codoped calcined at different temperatures (b), and (Fe, Cr)-codoped with different codoped concentration (c).

due to H₂ was produced on conduction band and O₂ was generated on valence band and some impurity states.

In XRD patterns the impurities phase which assigned to orthorhombic LaCrO₃ or Fe₃Ti₃O₁₀ appeared when Fe and Cr dopants concentration higher than 0.02 as well as the calcination temperature below 950 °C. The impurity phase resulted from the inhomogeneous substitution is very easily to introduce the crystal defects as electron–hole recombination centers, leading to a low photocatalytic H₂ and O₂ evolution.

Fig. 8 shows the photostability of NiO_x (0.5 wt%) loaded (Fe, Cr)–C₂-LTO-T₄ photocatalyst and (Fe, Cr)–C₄-LTO-T₄ photocatalyst, which is investigated in two consecutive runs of accumulatively 8 h. The average H₂ generation rate over NiO_x (0.5 wt%) loaded (Fe, Cr)–C₂-LTO-T₄ is about 284.32 μmol g⁻¹ h⁻¹ with an AQE of 1.93% in the first run of 8 h photocatalytic reaction, and then slightly declines to 258.294 μmol g⁻¹ h⁻¹ with an AQE of 1.75% in the second run. The performance degradation is not obvious, which confirms

(Fe, Cr)–C₂-LTO-T₄ photocatalyst with good stability. The O₂ evolution rate decreased remarkably, which was possibly because the metallic Ag from the AgNO₃ sacrificial reagent shielded the incident light. The crystal structures of NiO_x (0.5 wt%) (Fe, Cr)–C₂-LTO-T₄ (Fig. 9a) and (Fe, Cr)–C₂-LTO-T₄ (Fig. 9b) after 16 h of photoreaction are essentially similar to those of the unirradiated ones, and there is no obvious deviation in the peak locations, indicating the crystalline structure stability of the photocatalyst.

3.7. Photocurrent

To further investigate and understand the electrons transfer of (Fe, Cr)-codoped La₂Ti₂O₇ photocatalyst, the photocurrent experiments are performed with the photocatalysts loaded with 0.5 wt% of NiO_x cocatalyst under solar irradiation, as shown in Fig. 10. The photocurrent of pure La₂Ti₂O₇ photocatalyst is very low due to the large band gap (ca. 3.8 eV), while La₂Ti₂O₇ with optimized Fe and Cr

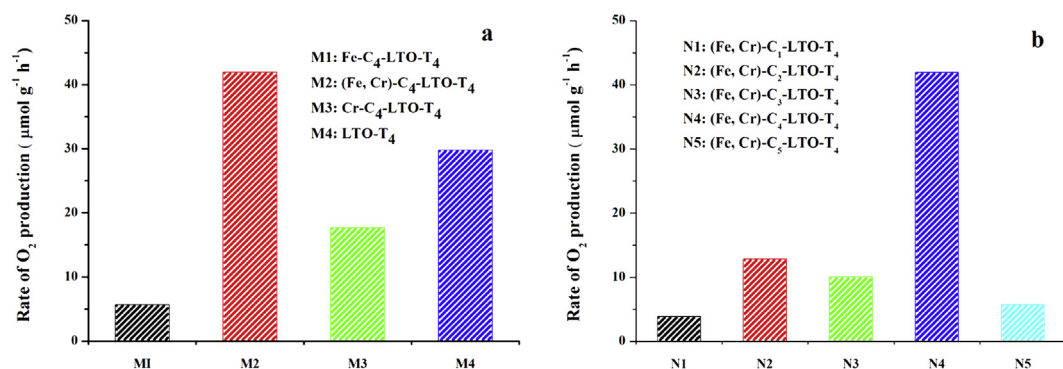


Fig. 7. Photocatalytic O₂ production of pure, monodoped and codoped (a) and (Fe, Cr)-codoped with different codoped concentration (b).

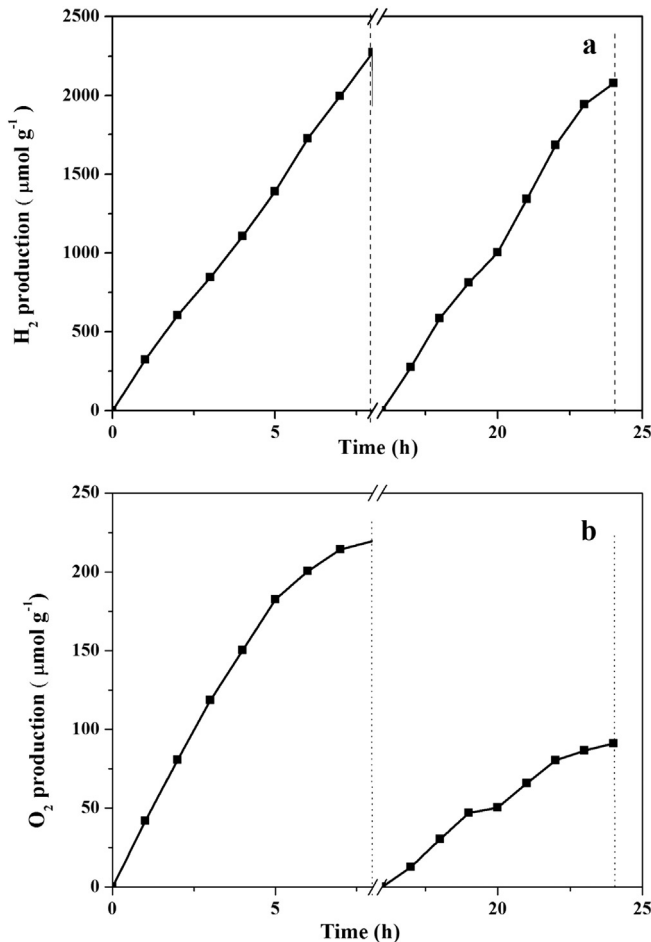


Fig. 8. Time courses of photocatalytic H_2 production over NiO_x (0.5 wt%) loaded (Fe, Cr)-C₂-LTO-T₄ and photocatalytic O_2 production over (Fe, Cr)-C₄-LTO-T₄.

codoping shows the highest photocurrent density of $177.39 \mu\text{A cm}^{-2}$. The high photocurrent of (Fe, Cr)-codoped La₂Ti₂O₇ photocatalysts means that more photoinduced electrons can transfer from the photocatalyst to the counter electrode via external circuit. And these results are in good agreement with the boosted photocatalytic H_2 production activity [5].

The high photocurrent and the excellent photocatalytic H_2 production activity of (Fe, Cr)-codoped La₂Ti₂O₇ photocatalyst may be ascribed to several reasons, including physical-chemical properties and synergistic effect of the codoping system. First of all, the physical-chemical properties, such as phase structure, crystallinity and morphology, are of great influence on the photocurrent and photocatalytic H_2 production activity. According to the above characterization analysis, (Fe, Cr)-codoped system prepared at high temperature could effectively improve the crystallinity and the homogeneity of the particle size, which can decrease the number of lattice defects that are easily to be the recombination center of photogenerated electrons and holes, leading to more photo-generated carriers to join in the reduction reaction. Secondly, Fe and Cr codoping into La₂Ti₂O₇ can result in the formation of wider impurity levels, leading to reduce the incident photon energy of electronic excitation to achieve indirect transition and further increase the degree of narrowing of band gap that help to absorb more solar light. Furthermore, the wider impurity levels are beneficial to the migration of carriers within the band gap of La₂Ti₂O₇ so as to reduce the recombination rate of photogenerated

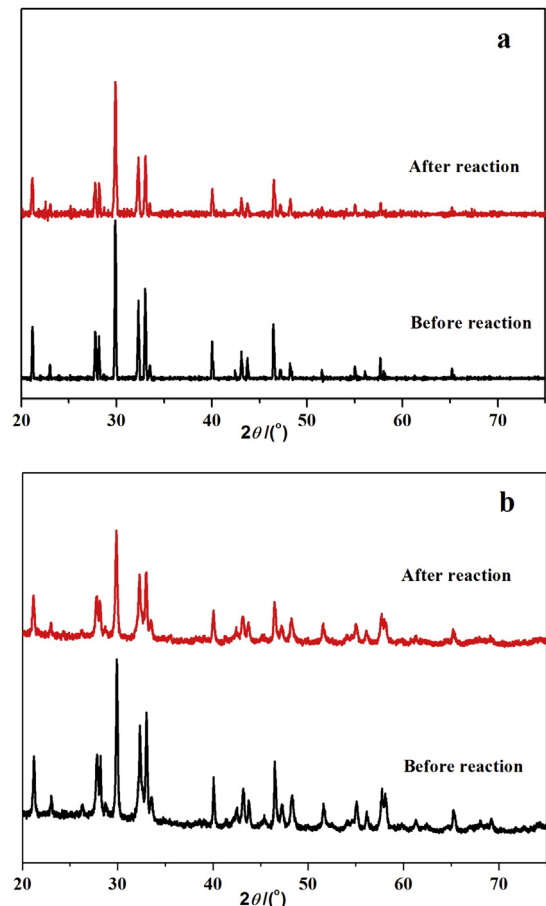


Fig. 9. XRD patterns of 0.5 wt% NiO_x loaded (Fe, Cr)-C₂-LTO-T₄ (a) and (Fe, Cr)-C₄-LTO-T₄ (b) before and after 16 h of photocatalytic H_2 evolution reaction.

electrons and holes. However, it is worth noting that high codoped concentration may induce abundant crystal defects as electron-hole recombination centers, causing a sharp decrease of photocatalytic H_2 production activity.

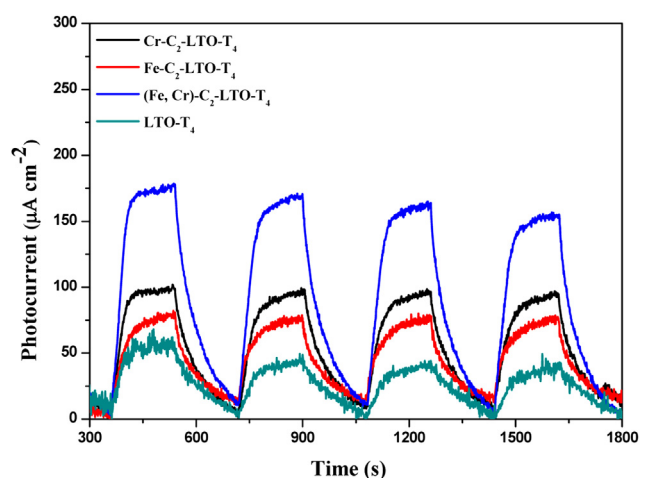


Fig. 10. Photocurrent-time ($I-t$) curves of pure, monodoped and (Fe, Cr)-codoped La₂Ti₂O₇ photocatalysts under simulated solar light in 1 M Na₂SO₄ aqueous solution. Voltage: 0.5 V.

4. Conclusions

$\text{La}_2\text{Ti}_2\text{O}_7$ codoped with Fe and Cr is prepared by sol–gel method and characterized of crystal phase, morphology, optical absorption property and H_2 production activity in detail. The results demonstrate that structural properties and photocatalytic H_2 production activities are strongly affected by the calcination temperature and codopant concentration. The synergistic effects of Fe and Cr codoping could further narrow the band gap and reduce the recombination rate of photogenerated electrons and holes, and enhance the optical absorption capacity and efficient photocatalytic activity for H_2 production by water splitting. $\text{La}_2\text{Ti}_2\text{O}_7$ codoped with 0.005 Fe and Cr calcined at 1150 exhibits the high photocatalytic H_2 production activity compared to the undoped or monodoped samples. The results show that (Fe, Cr)-codoping is a feasible way for enhancing $\text{La}_2\text{Ti}_2\text{O}_7$ photocatalytic H_2 production activity.

Acknowledgments

This work is supported by National Natural Science Foundation of China (50902056). The authors would like to thank Materials Characterization Center of Huazhong University of Science and Technology for XRD, FSEM and XPS assistance.

References

- [1] A. Fujishima, K. Honda, *Nature* 238 (1972) 37–38.
- [2] A.J. Bard, M.A. Fox, *Acc. Chem. Res.* 28 (1995) 141–145.
- [3] S. Dunn, *Int. J. Hydrogen Energy* 27 (2002) 235–264.
- [4] M.S. Zhu, Y.K. Du, P. Yang, X.M. Wang, *Catal. Sci. Technol.* 3 (2013) 2295–2302.
- [5] M.S. Zhu, Y.P. Dong, Y.K. Du, Z.G. Mou, J. Liu, P. Yang, X.M. Wang, *Chem. Eur. J.* 18 (2012) 4367–4374.
- [6] M.S. Zhu, Y.T. Lu, Y.K. Du, J. Li, P. Yang, X.M. Wang, *Int. J. Hydrogen Energy* 36 (2011) 4298–4304.
- [7] T. Takata, Y. Furumi, K. Shinohara, A. Tanaka, M. Hara, J.N. Kondo, K. Domen, *Chem. Mater.* 9 (1997) 1063–1064.
- [8] H.G. Kim, D.W. Hwang, J. Kim, Y.G. Kim, J.S. Lee, *Chem. Commun.* (1999) 1077–1078.
- [9] K.I. Yeong, S. Samer, J.H. Munir, E.M. Thomas, *J. Am. Chem. Soc.* 113 (1991) 9561–9563.
- [10] C.H. Wu, Y.Z. Zhang, S. Lia, H.J. Zheng, H. Wang, J.B. Liu, K.W. Li, H. Yan, *Chem. Eng. J.* 178 (2011) 468–474.
- [11] R. Wang, D. Xu, J.B. Liu, K.W. Li, H. Wang, *Chem. Eng. J.* 168 (2011) 455–460.
- [12] D.W. Hwang, H.G. Kim, J.S. Jang, S.W. Bae, S.M. Ji, J.S. Lee, *Catal. Today* 93–95 (2004) 845–850.
- [13] Z.H. Li, H. Xue, X.X. Wang, X.Z. Fu, *J. Mol. Catal. A Chem.* 260 (2006) 56–61.
- [14] D. Logvinovich, A. Börger, M. Döbelic, S.G. Ebbinghausd, A. Rellerd, A. Weidenkaff, *Prog. Solid State Chem.* 35 (2007) 281–290.
- [15] J.L. Sotelo, G. Ovejeroa, J.A. Melerob, A. Milenia, *Appl. Catal. B Environ.* 47 (2004) 281–294.
- [16] D.W. Hwang, H.G. Kim, J.S. Lee, J. Kim, W. Li, S.H. Oh, *J. Phys. Chem. B* 109 (2005) 2093–2102.
- [17] R. Long, N.J. English, *Phys. Chem. Chem. Phys.* 13 (2011) 13698–13703.
- [18] Y.M. Lin, Z.Y. Jiang, C.Y. Zhu, X.Y. Hu, H.Y. Zhu, X.D. Zhang, J. Fan, S.H. Lin, *Int. J. Hydrogen Energy* 38 (2013) 5209–5214.
- [19] Q.Z. Wang, N. An, W. Chen, R.F. Wang, F.P. Wang, Z.Q. Lei, W.F. Shangguan, *Int. J. Hydrogen Energy* 37 (2012) 12886–12892.
- [20] L. Lin, Y.C. Chai, Y.C. Yang, X. Wang, D.N. He, Q.W. Tang, S. Ghoshroy, *Int. J. Hydrogen Energy* 38 (2013) 2634–2640.
- [21] H. Yu, S.C. Yan, Z.S. Li, T. Yu, Z.G. Zou, *Int. J. Hydrogen Energy* 37 (2012) 12120–12127.
- [22] H.J. Zhang, G. Chen, X.D. He, J. Xu, *J. Alloys Compd.* 516 (2012) 91–95.
- [23] A.Z. Jia, X.Q. Liang, Z.Q. Su, T. Zhu, S.X. Liu, *J. Hazard. Mater.* 178 (2010) 233–242.
- [24] M. Sathish, R.P. Viswanath, *Catal. Today* 129 (2007) 421–427.
- [25] S.K. Lee, P.K.J. Robertson, A. Mills, D. McStay, N. Elliott, D. McPhail, *Appl. Catal. B Environ.* 44 (2003) 173–184.
- [26] H. Tada, S. Tsuji, S. Ito, *J. Colloid Interface Sci.* 239 (2001) 196–199.
- [27] K. Inumaru, M. Murashima, T. Kasahara, S. Yamanaka, *Appl. Catal. B Environ.* 52 (2004) 275–280.
- [28] M.M. Milanoval, M. Kakihana, M. Arima, M. Yashima, M. Yoshimura, *J. Alloys Compd.* 242 (1996) 6–10.
- [29] Z.H. Li, G. Chen, X.J. Tian, Y.G. Li, *Mater. Res. Bull.* 43 (2008) 1781–1788.
- [30] K.W. Li, Y. Wang, H. Wang, M.K. Zhu, H. Yan, *Nanotechnology* 17 (2006) 4863–4867.
- [31] D.W. Hwang, K.Y. Cha, J. Kim, H.G. Kim, S.W. Bae, J.S. Lee, *Ind. Eng. Chem. Res.* 42 (2003) 1184–1189.
- [32] M.S. Zhu, P.L. Chen, M.H. Liu, *J. Mater. Chem.* 21 (2011) 16413–16419.
- [33] M.S. Zhu, Z. Li, B. Xiao, P. Yang, X.M. Wang, *ACS. Appl. Mater. Interfaces* 5 (2013) 1732–1740.
- [34] D. Wang, J. Ye, T. Kako, T. Kimura, *J. Phys. Chem. B* 110 (2006) 15824–15830.
- [35] Y. Qin, G. Wang, Y. Wang, *Catal. Commun.* 8 (2007) 926–930.
- [36] S. Bouattour, A.M.B. Regob, L.F.V. Ferreira, *Mater. Res. Bull.* 45 (2010) 818–825.
- [37] V.G. Bessergenev, R.J.F. Pereira, M.C. Mateus, I.V. Khmelinskii, D.A. Vasconcelos, R. Nicula, E. Burkel, A.M. Botelho do Rego, A.I. Saprykin, *Thin Solid Films* 503 (2006) 29–39.
- [38] Q.C. Xu, D.V. Wellia, S. Yan, D.W. Liao, T.M. Lim, T.T.Y. Tan, *J. Hazard. Mater.* 188 (2011) 172–180.
- [39] Y.F. Lee, K.H. Chang, C.C. Hu, K.M. Lin, *J. Mater. Chem.* 20 (2010) 5682–5688.
- [40] M.F. Sunding, K. Hadidi, S. Diplas, O.M. Løvvik, T.E. Norby, A.E. Gunnæs, *J. Electron Spectrosc. Relat. Phenom.* 184 (2011) 399–409.
- [41] M. Yang, L.H. Huo, H. Zhao, S. Gao, Z.M. Rong, *Sens. Actuators B Chem.* 143 (2009) 111–118.
- [42] X.Q. Cheng, Z.C. Feng, C.T. Li, C.F. Dong, X.G. Li, *Electrochim. Acta* 56 (2011) 5860–5865.
- [43] W. Zhang, Y. Li, S. Zhu, F. Wang, *Chem. Phys. Lett.* 373 (2003) 333–338.
- [44] K.K. Kartha, M.R. Pai, A.M. Banerjee, R.V. Pai, S.S. Meena, S.R. Bharadwaj, *J. Mol. Catal. A Chem.* 335 (2011) 158–168.
- [45] M. Ghaffaria, T. Liu, H. Huang, O.K. Tan, M. Shannon, *Mater. Chem. Phys.* 136 (2012) 347–357.
- [46] C. Gargori, S. Cerro, R. Galindo, A. García, M. Llusr, G. Monrós, *Ceram. Int.* (2012) 4453–4460.
- [47] H. Kato, A. Kudo, *J. Phys. Chem. B* 106 (2002) 5029–5034.
- [48] P.E. Blochl, *Phys. Rev. B Condens. Matter* 50 (1994) 17953–17979.
- [49] G. Kresse, J. Hafner, *Phys. Rev. B Condens. Matter* 47 (1993) 558–561.
- [50] G. Kresse, J. Hafner, *Phys. Rev. B Condens. Matter* 49 (1994) 14251–14269.
- [51] G. Kresse, D. Joubert, *Phys. Rev. B Condens. Matter Mater. Phys.* 59 (1999) 1758–1775.
- [52] S.L. Dudarev, G.A. Botton, S.Y. Savarsov, C.J. Humphreys, A.P. Sutton, *Phys. Rev. B* 57 (1998) 1505–1509.